ALEPH 91-40
PHYSIC 91-38
S. Roehn, A. Stahl
18.3.1991

Measurements of τ Production and Decay Parameters from the combined Energy/Angle Distribution of μ from $\tau \longrightarrow \mu\,\nu_\tau\nu_\mu$ Decays

Steffen Roehn
Institut für Physik, Universität Mainz

Achim Stahl
Institut für Hochenergiephysik, Universität Heidelberg

March 12, 1991

Abstract

Based on the data taken in 1989 and 1990, 1509 $\tau \rightarrow \mu\,\nu_\tau\nu_\mu$ decays are selected to measure the combined momentum/angle spectrum of the μ. From this distribution three sets of parameters have been extracted:

(1) The simultaneous determination of

$\frac{g_{v_e}(s=M_Z^2)}{g_{a_e}(s=M_Z^2)} = 0.110 \pm 0.059_{stat} \pm 0.019_{syst}$ and

$\frac{g_{v_\tau}(s=M_Z^2)}{g_{a_\tau}(s=M_Z^2)} = 0.119 \pm 0.057_{stat} \pm 0.031_{syst}$.

(2) The measurement of

$\frac{g_{v_{lepton}}(s=M_Z^2)}{g_{a_{lepton}}(s=M_Z^2)} = 0.114 \pm 0.032_{stat} \pm 0.016_{syst}$ assuming lepton universality.

(3) The simultaneous determination of the τ decay parameter

$\xi = 0.72\,^{+0.52}_{-0.34}{}_{stat} \pm 0.30_{Uncert.\,on\,g_{v_e},\rho} \pm 0.18_{syst}$ and

$\frac{g_{v_\tau}(s=M_Z^2)}{g_{a_\tau}(s=M_Z^2)} = 0.201 \pm 0.071_{stat}\,^{+0.154}_{-0.056}{}_{Uncert.\,on\,g_{v_e},\rho} \pm 0.015_{syst}$

using the constraint from the forward–backward asymmetry measurement in the τ channel. This is the first measurement of the parameter ξ in τ decays.

Furthermore Monte Carlo studies on the sensitivity to the other decay parameters ρ and δ have been performed.

1 Introduction

Energy and polar angle ($cos\theta$) of μ's from $\tau \rightarrow \mu\,\nu_\tau\nu_\mu$ decays contain information about the couplings g_{v_e} and g_{a_e} of the initial state, the couplings g_{v_τ} and g_{a_τ} of the final state and the Lorentz structure of the decay of the $\tau \rightarrow \mu\,\nu\,\nu$. These informations from the two–dimensional energy/angle distribution go beyond the ones which can be extracted from the energy distribution alone as done in [2]. Nevertheless, the basic techniques concerning selection of events, determination of background and systematics are the same as described in [2]. Therefore only the changes and improvements compared to this reference are explained and the interested reader is asked to refer to this note.

In this note particular emphasis is put on the different observables which can be extracted from the combined energy/angle distribution.

2 Main Changes compared to Energy Analysis

(i) A correct treatment of the **angular information** of the μ from τ decays implies the knowledge of the systematics in energy *and* $cos\theta$ of the charged track. To take these effects into account, the detector is separated into five "$cos\theta$" bins as given in table 1. The analysis as described in [2] is performed as function of energy separately in each of those angular bins. This separation in bins follows closely the 'natural' definition given by the different HCAL parts (endcap, overlap and barrel), because HCAL is the main component for signal identification and background suppression. Clearly the number of events is quite different for the individual detector bins. So, the number of bins in the momentum spectra for the different $cos\theta$ regions are chosen appropriately. This is indicated in table 1, where the number of bins for the momentum range from 0. to 1.0 is given as well.

(ii) The **μ–identification** has been improved by using a different variable for π rejection keeping the background of π nearly constant.

Detector	Angular Range	Number of momentum bins for $0. \leq x \leq 1.$
ENDCAP A	$0.7 < cos\theta \leq 0.9$	10
OVERLAP A	$0.6 < cos\theta \leq 0.7$	5
BARREL	$-0.6 \leq cos\theta \leq 0.6$	20
OVERLAP B	$-0.7 \leq cos\theta < -0.6$	5
ENDCAP B	$-0.9 \leq cos\theta < -0.7$	10

Table 1: *Angular and momentum bins in the analysis*

(iii) The cuts on **acolinearity**, x_{recoil} and **LCAL energy** have been changed marginally.

3 Selection and Background

3.1 Cuts for Selection

A good track is is defined as follows:

At least 4 TPC hits,
Momentum larger than 0.1 GeV/c,
$z_0 < 10cm$, and
$d_0 < 2cm$.

Based on these good tracks the event is divided into two hemispheres using the thrust axis. The following cuts are applied:

E.1	At least 2 good tracks in the event.
E.2	Not more than 6 good tracks in the event.
E.3	At least 1 good track per hemisphere.
E.4	The cosine of the angle between the two jets is below -0.95 (Acolinearity).
E.5	There is less than 5 GeV of total 'wire' energy in LCal.

Looking now at the individual tracks, a good μ is defined as:

S.1	No further good track in that hemisphere.
S.2	$x_\mu = \frac{p_\mu}{E_{Beam}} > 0.1$.
S.3	$\|cos(\theta)\| < 0.9$, where θ is the angle of the μ w.r.t the beam line.
S.4	μ–identification as described in the section 3.2.

To reject most of the background from $Z_0 \rightarrow \mu^+\mu^-$, the following cuts are applied on the recoil side:

R.1	$x_{recoil} = \frac{p_{recoil}}{E_{Beam}} < 0.77$.
R.2	no μ–pre–identification (as described in section 3.2) for the recoil side.

A good event is defined by demanding all cuts mentioned in this section.

3.2 μ Identification

For the identification of μ the usual penetration cut together with a cut on the mean number of clusters per fired plane in HCAL (CLPPLN) is used. The last one provides better μ/π separation as the one used in [2]. Figure 1 shows the CLPPLN distribution

	Overall	Endcap B	Overlap B	Barrel	Overlap A	Endcap A
$\epsilon_{\mu-ID}$	91.5 ± 0.8	93.3 ± 1.2	88.4 ± 1.6	91.4 ± 0.6	83.4 ± 1.5	93.3 ± 1.2
$\epsilon_{\mu-pre-ID}$	95.7 ± 0.6	97.3 ± 0.5	95.5 ± 1.2	95.2 ± 0.5	93.3 ± 0.9	97.4 ± 1.1

Table 2: Efficiencies for μ–identification in percent

for the barrel region ($|cos\theta| \leq 0.6$) and the endcap/overlap region ($0.6 < |cos\theta| \leq 0.9$). The following criteria are used to define a μ:

M.1	Penetration		in last ten planes:
			At least 2 fired planes
		and	$NUMBER\ OF\ EXPECTED\ FIRED\ PLANES \geq 1$
		and	$\frac{NUMBER\ OF\ FIRED\ PLANES}{NUMBER\ OF\ EXPECTED\ FIRED\ PLANES} \geq 0.4$
			road used: $2cm + 3\sigma_{M.S.}$.
M.2	Mean number of clusters per fired plane		in all planes
			in *Barrel*: $CLPPLN < 1.3$
			in *Endcap*: $CLPPLN < 1.4$
			road used: $30cm + 3\sigma_{M.S.}$.

To reject events like $Z_0 \rightarrow \mu^+\mu^-$, the μ–pre–identification is given by (in the last ten planes):

PR.1	Penetration	$\frac{NUMBER\ OF\ FIRED\ PLANES}{NUMBER\ OF\ EXPECTED\ FIRED\ PLANES} \geq 0.2$, if at least one plane is expected to fire, or $NUMBER\ OF\ FIRED\ PLANES \geq 1$ otherwise.

The corresponding efficiencies measured via the pair–tag method (testsample 2 in [2]) for the different detector bins are shown in table 2 (the slope is measured via the chamber–tag method; testsample 1 in [2]). The systematic error is already included. The dependence on momentum in the different bins are shown in figure 2 for the μ–identification and in figure 3 for the μ–pre–identification.

3.3 Acceptance and Resolution

The Monte Carlo is used to get the acceptance and the resolution in momentum and angle. For this calculation all cuts but S4 (μ–identification) are applied. The acceptance is obtained by dividing the number of accepted events in a momentum/$cos\theta$ bin by the number of generated events in the same bin.

Detector	average Acceptance in %	Slope of momentum dependence in %
ENDCAP B	70.6 ± 0.7	5.7 ± 4.3
OVERLAP B	76.4 ± 1.0	16.5 ± 6.0
BARREL	73.5 ± 0.3	2.3 ± 2.5
OVERLAP A	73.3 ± 1.1	0.3 ± 6.1
ENDCAP A	70.4 ± 0.7	10.8 ± 4.5

Table 3: *Acceptance (height and slope)*

The corresponding average acceptance for each detector region is shown in the first column of table 3. One can see a significant drop of the acceptance in the endcaps. This is mainly due to the cut in $|cos\theta|$ of a track together with cut E.3, demanding at least one track in each hemisphere: A track is not only cut because of it's own $cos\theta$, but also if the recoiling track is out of the angular range, which happens mainly in the endcaps.

The acceptance as a function of momentum is shown in figure 4 together with a straight line fit. As the bins in the region [0.9,0.95] for the barrel and [0.9,1.0] for the endcaps are off (due to resolution effects), they are excluded from this straight line fit. To be compatible in the overlap, the bin in the region [0.8,1.0] has been excluded there. The results are shown in the second column of table 3. Clearly, the restriction to [0.1,0.9] or [0.1,0.8] is only made to get the slope of the acceptance properly. The remaining bin is not excluded for the final fit.

To correct for the acceptance effects, the values given in table 3 are used to define an efficiency function $\epsilon_{Acceptance}(x, cos\theta)$ for the region [0.1,0.9] in the barrel and the endcaps and for [0.1,0.8] in the overlap regions. The correction for the remaining bin is taken as the acceptance in this bin as shown in figure 4.

3.4 Background

The significant background contributions ([2]) are from $\tau^{\pm} \rightarrow hadron^{\pm}\,\nu \geq 0\,neutrals$, from μ–pairs and from the 2 photon process.

3.4.1 $\tau^{\pm} \rightarrow hadron^{\pm}\,\nu \geq 0\,neutrals$

The π^0–tag method (testsample 4 in [2]) is used to define a clean sample of charged π. The corresponding misidentification probability (to identify a π as a μ) versus momentum for the whole detector is shown in figure 5. This plot is used to fit a slope w.r.t. momentum, which gives $(-1.5 \pm 1.8)\%$. Due to lack of statistics the slope has been fitted for the whole detector only. This slope is used for all detector bins, while the absolute height ϵ_{π}^{0} is taken from the individual detector regions. Those misidentification probabilities are shown in table 4.

To correct for the background, the following procedure is applied: Those τ decays resulting in one charged π with an arbitrary number of neutral particles are selected in the Monte Carlo. Then all cuts except the μ–identification (S.4) are applied. The resulting spectra are scaled by

	Endcap B	Overlap B	Barrel	Overlap A	Endcap A
ϵ_π^0 in %	0.4 ± 0.4	0	1.1 ± 0.4	2.5 ± 1.7	1.8 ± 0.9
Events *hadron* bckgrd.	1.7	0	24.6	7.9	5.8
Events μ-pair bckgrd.	4.4	2.6	29.5	3.2	4.1

Table 4: π misidentification probability and number of background events for *hadron* and μ-pair background

$$\frac{N^i_{\mu,data,after\,all\,cuts}}{\epsilon^i_{\mu-Id}} \times \frac{N^i_{\pi,MC,after\,cuts}}{N^i_{\mu,MC,after\,cuts}}, \tag{1}$$

where i refers to the momentum/angular bin and "after cuts" means all cuts except μ–identification. These spectra have to be scaled with the π misidentification probability. Hence, they are multiplied with the linear function consisting of ϵ_π^0 of the relevant detector region and the overall slope. The corresponding background spectra are shown in figure 6. The total number of background events is given in table 4 as well.

Finally these spectra are related to the signal to give the correction function $\epsilon_\pi(x, cos\theta)$.

3.4.2 μ–Pairs

The μ–pre–identification is used to define the momentum dependence of the background in the different detector bins. This is done by demanding the μ–pre–identification in each hemisphere using the cuts for the signal except S.4 and R.2, clearly. Then this distribution is scaled by a factor

$$\frac{1 - \epsilon_{\mu-pre-ID}}{\epsilon^2_{\mu-pre-ID}}\ \epsilon_{\mu-ID}. \tag{2}$$

The corresponding distributions are shown in figure 7, while the number of background events are shown in table 4.

For the final correction these distributions are divided by the signal to give $\epsilon_{\mu\mu}(x, cos\theta)$.

3.4.3 Two–Photon Process

In principle the events of the type $e^+e^- \rightarrow e^+e^-\mu^+\mu^-$ should be already subtracted as explained in subsection 3.4.2. This is only partially the case for the process $e^+e^- \rightarrow e^+e^-\tau^+\tau^-$. To give an upper limit of the number of events not taken into account, the acolinearity region from -0.8 to 0. in data is used as a control region to get an estimate of the number of events in the signal region. In this region 32 events in the data are found out of which 4 come from radiative τ decays estimated from Monte Carlo. The remaining 28 events are multiplied with the ratio of events in signal and control region determined by Monte Carlo ($\approx$ 25%). This leads to 7 background events in the signal region for the whole detector. As μ's from the 2 photon process are predominantly at low energies and high $|cos\theta|$, those seven events are distributed for systematic studies in the lowest energy bin in the individual detectors. To take the angular dependence into account, 2

are assumed to be in each endcap, 1 in each overlap and 1 in the barrel. This is an upper limit on the remaining background, because some of this 7 events are subtracted with the μ–pair correction.

3.5 Final Spectra

The final spectra in the different detector bins are shown in figure 8.

4 Fitting Method

To extract the maximal information about the τ couplings to the Z^0 and the Lorentz structure of the decay both the μ momentum and the angle of the μ w.r.t. the beam direction are taken into account. Below the basic equations are given and explained. The strategy is based on [3] and more detailed information can be found in [1].

4.1 Basic formulas and Measurements on the Born–level

On the tree level the cross–section for the production of $\tau^+\tau^-$ pairs is given by [3]

$$\begin{aligned}\frac{d\sigma^{Born}}{dcos\theta}(P_{\tau^-};s,cos\theta) &= \Big[(1+cos^2\theta)F_0(s)+2cos\theta F_1(s)\Big] - \\ &\quad \Big[(1+cos^2\theta)F_2(s)+2cos\theta F_3(s)\Big]\,P_{\tau^-}, \end{aligned} \tag{3}$$

where θ is the angle of the outgoing τ^- relative to the incoming e^-, s the center–of–mass energy squared ($s = 4E^2_{Beam}$) and P_{τ^-} the helicity (± 1) of the τ^-. The F_i are given by

$$\begin{aligned}
F_0(s) &= \frac{G_F^2\,M_Z^4\,\rho_0^2}{32\,\pi\,s}|\chi(s)|^2(g_{v_e}^2+g_{a_e}^2)(g_{v_\tau}^2+g_{a_\tau}^2)+\frac{\sqrt{2}\,G_F\,M_Z^2\,\rho_0}{16\,s}2\,Re\{\alpha^*\chi(s)\}q_eq_\tau g_{v_e}g_{v_\tau} \\
&\quad +\frac{\pi\,|\alpha|^2}{4\,s}q_e^2q_\tau^2 \\
F_1(s) &= \frac{G_F^2\,M_Z^4\,\rho_0^2}{32\,\pi\,s}|\chi(s)|^2 2g_{v_e}g_{a_e}2g_{v_\tau}g_{a_\tau}+\frac{\sqrt{2}\,G_F\,M_Z^2\,\rho_0}{16\,s}2\,Re\{\alpha^*\chi(s)\}q_eq_\tau g_{a_e}g_{a_\tau} \\
F_2(s) &= \frac{G_F^2\,M_Z^4\,\rho_0^2}{32\,\pi\,s}|\chi(s)|^2(g_{v_e}^2+g_{a_e}^2)2g_{v_\tau}g_{a_\tau}+\frac{\sqrt{2}\,G_F\,M_Z^2\,\rho_0}{16\,s}2\,Re\{\alpha^*\chi(s)\}q_eq_\tau g_{v_e}g_{a_\tau} \\
F_3(s) &= \frac{G_F^2\,M_Z^4\,\rho_0^2}{32\,\pi\,s}|\chi(s)|^2 2g_{v_e}g_{a_e}(g_{v_\tau}^2+g_{a_\tau}^2)+\frac{\sqrt{2}\,G_F\,M_Z^2\,\rho_0}{16\,s}2\,Re\{\alpha^*\chi(s)\}q_eq_\tau g_{a_e}g_{v_\tau},
\end{aligned} \tag{4}$$

$$\chi(s) = \frac{s}{s-M_Z^2+is\Gamma_Z/M_Z}. \tag{5}$$

Two different coupling strengths are used: α and $\sqrt{2}G_F M_Z^2 \rho_0$. They describe the photon and Z^0 exchange, respectively. Even though the Standard Model gives a precise relation between them:

$$\frac{4\pi\alpha}{4\,sin^2\theta_W\,cos^2\theta_W} = \sqrt{2}\,G_F\,M_Z^2\,\rho_0, \tag{6}$$

they are kept separate. This will be very useful for the treatment of radiative corrections. For the same reason, α is used as a complex number (α^* is the complex conjugate of α). The imaginary part of the propagator $\chi(s)$ takes the finite width of the Z^0 into account. ρ_0 should not be confused with the Michel parameter ρ; ρ_0 describes the Higgs structure of the Standard Model. For the case of a Higgs doublet, it is 1 (this shall be assumed throughout this note). Furthermore the coupling constants g_{v_i} and g_{a_i} of the leptons ($i = e, \mu, \tau$) to the Z^0 play an important role. The Standard Model prediction for them is given by

$$\begin{aligned} g_{a_i} &= I_3^i \\ g_{v_i} &= I_3^i - 2Q_i sin^2\theta_W. \end{aligned} \tag{7}$$

Looking at the peak only ($s = M_Z^2$), equation (3) simplifies to

$$\begin{aligned} \frac{d\sigma^{Born}}{dcos\theta}(P_{\tau^-}; s = M_Z^2, cos\theta) \;\propto\; & \Big[(1 + cos^2\theta) + 2cos\theta A_e A_\tau\Big] - \\ & \Big[(1 + cos^2\theta)A_\tau + 2cos\theta A_e\Big]\, P_{\tau^-}, \\ A_i \;=\; & \frac{2g_{a_i}g_{v_i}}{g_{a_i}^2 + g_{v_i}^2}. \end{aligned} \tag{8}$$

Therefore equation (8) is sensitive to the ratios A_i only—not to the couplings themselves. It is straightforward to extract the asymmetries $A_{FB} = 3/4\,A_e\,A_\tau$, $A_{pol} = -A_\tau$ and $A_{pol}^{FB} = -A_e$ from this formula by integrating/summing in particular ways over the angle/polarisation (see e.g. [3]). While A_{FB} and A_{pol} are well known, A_{pol}^{FB} is the mean polarisation of τ^- in the forward direction minus the mean polarisation in the backward direction divided by the sum of the two. Those asymmetries are not measured in this analysis. Instead the whole equation (3) is used to extract A_e and A_τ directly.

Before regarding the possibility of measuring A_e and A_τ, the subsequent decay has to be taken into account. All formulas given for the decay $\tau \to \mu\,\nu\,\nu$ are valid for the electron channel as well. The decay rate is given by the most general decay formula given in [9] as a function of $x = E_\mu/E_\tau$:

Parameter	*Predictions*		*Measurements*
	$(V-A)_{\tau,\mu}$	$(V+A)_{\tau,\mu}$	
Michel Parameter ρ	3/4	3/4	0.731 ± 0.030 [10]
Low energy Parameter η	0	0	none
Asymmetry Parameter ξ	+1	−1	none
Asymmetry Parameter δ	3/4	3/4	none

Table 5: *Predictions and measurements of τ decay parameters*

$$\begin{aligned}
\frac{d\Gamma(x)}{dx} &= \frac{m_\tau^5 {G_F}^2}{32\pi^3} h^\mu(x;\xi P_{\tau^-},\rho,\delta), \\
\text{with } h^\mu(x;\xi P_{\tau^-},\rho,\delta) &= \left[h_0^\mu(x;\rho) - \xi P_{\tau^-}\, h_1^\mu(x;\delta)\right], \\
, h_0^\mu(x;\rho) &= 2 - 6x^2 + 4x^3 + \frac{4}{9}\rho(-1 + 9x^2 - 8x^3) \\
h_1^\mu(x;\delta) &= -\frac{2}{3} + 4x - 6x^2 + \frac{8}{3}x^3 + \frac{4}{9}\delta(1 - 12x + 27x^2 - 16x^3). \quad (9)
\end{aligned}$$

Here the decay parameters ρ, ξ and δ describing the Lorentz structure of the decay are kept within the formula[1]. Their definition can be found in [9]. Assuming only vector and axialvector couplings to be present in the charged current mechanism of the τ decay, the predictions and measurements carried out so far are given in table 5. It is worth noting that the decay rate (equation 9) is not sensitive to the polarisation P_{τ^-} of the τ alone, but to the product of ξP_{τ^-}.

The last step is to combine the production of the τ (equation 3) with the decay (equation 9), which leads to (dropping all constant factors):

$$\begin{aligned}
\frac{d^2\sigma^{Born}}{dcos\theta\, dx}(s, cos\theta, x) &= \frac{d\sigma^{Born}}{dcos\theta}(P_{\tau^-} = +1, s, cos\theta)\left[h_0^\mu(x;\rho) - \xi\, h_1^\mu(x;\delta)\right] + \\
&\quad \frac{d\sigma^{Born}}{dcos\theta}(P_{\tau^-} = -1, s, cos\theta)\left[h_0^\mu(x;\rho) + \xi\, h_1^\mu(x;\delta)\right] \\
&\propto \left\{(1 + cos^2\theta)F_0(s) + 2cos\theta F_1(s)\right\} h_0^\mu(x;\rho) + \\
&\quad \left\{(1 + cos^2\theta)F_2(s) + 2cos\theta F_3(s)\right\} \xi\, h_1^\mu(x;\delta). \quad (10)
\end{aligned}$$

[1]The parameter η is lost, because a term $x_0^\star\eta$, where $x_0^\star = \frac{m_\mu}{E_\mu^{cms,max}} = 0.117$, has been neglected, see [1].

The result is a formula which describes the cross–section in terms of the polar angle of the τ and the momentum of the τ decay product. It is thereby sufficient to use the angle of the decay product instead of the unknown angle of the τ (see [1]). One is now able to use the whole information available from a track to extract different parameters from equation (10). This is done by a fit of the combined momentum/$cos\theta$ spectrum of the μ's to this equation. Doing this, the energy range has to be reduced to [0.1;0.95], because equation (10) is not valid at the edges of the spectrum (see [1]). Nevertheless this accounts for a very small loss in sensitivity. Furthermore the experimental circumstances require a minimal energy cut anyway.

4.2 Different Measurements

To explain the basic measurements it is enough to regard equation (10) on the peak (use $F_i(s = M_Z^2)$):

- *A Measurement of the Production Parameters* A_e and A_τ can be obtained by assuming "V-A" in the decay process. Using the angular and momentum information allows then to be sensitive to A_e, A_τ and the product A_eA_τ (instead of A_τ only without angular information). It should be stressed that the sensitivity to A_τ itself becomes higher using the angular information because of the correlation between A_e and A_τ due to the term $2cos\theta A_eA_\tau$. For the case of lepton universality the 2–dimensional distribution clearly gives a much better sensitivity to A_{lepton} than a polarisation measurement only. More quantitative statements will be given in subsection 4.4.

- *A Measurement of the Decay Parameters* ρ, ξ and δ. For this purpose the production parameters are fixed to their value given by the measured forward–backward asymmetries and the width of the electron and τ channel. Then equation (10) depends on three parameters. The best way would be to extract them simultaneously. Unfortunately the statistics is at the present stage too poor for this task. To demonstrate the sensitivity w.r.t. the single parameters (e.g. for comparison with the correlation formalism) results are given in subsection 4.4 on Monte Carlo.

- *A Measurement of One Decay Parameter and One Production Parameter.* This is of particular interest, as the relevant quantities of the τ production and decay should be measured together. Hereby it is necessary again to concentrate on some interesting parameters. As ρ is measured quite accurately by [10], it is fixed to it's measured value, while ξ and δ have not been measured so far at all. Looking at the possibility of "V-A" or "V+A" at both vertices of the W in the τ decay, ρ and δ have in both cases the value 3/4, while ξ is either 1 ("V–A") or -1 ("V+A"). Therefore A_τ and ξ are chosen to be measured simultaneously. To incorporate the measurement of A_τ from the forward-backward asymmetry in the τ channel as well, it's measurement is used as a constraint in the fit.

4.3 Radiative Corrections

Radiative corrections contribute significantly to the shape of the spectra. Two different corrections have to be regarded (see [4]):

(i) "QED corrections". They consist of all one–loop diagrams with an extra real photon or a virtual photon loop. As they form a gauge invariant subset and depend on the experimental cuts, it is sensible to separate them from the

(ii) "weak corrections". They consist of all the other possible one–loop diagrams as modifications of the propagator for γ, Z^0, vertex corrections and box diagrams with two massive boson exchange.

The "weak corrections" can be separated into different effects (see [4, 5, 6]):

(i) *The Real Part and Imaginary Part of the Propagator Corrections* can be taken into account by introducing s–dependent coupling constants. The tree level expressions can be used with these new coupling constants (the dependence on s is important only for $\alpha(s)$). As there are three different contributions (Z–loop–Z, Z–loop-γ and γ–loop–γ), three constants are needed to absorb them. The Real Part of the *Z–loop–Z* contribution leads to a redefinition of ρ_0 into a $\rho(s)$. The imaginary part of those corrections can be absorbed into the physical (thus observable) width Γ_Z, leading to the complex $\chi(s)$ as given in equation (5). The *Z–loop–γ* part can be taken into account by a redefinition of $sin^2\theta_W$ into $sin^2\theta_W(s)$. Hereby the imaginary part is neglected. This redefinition of $sin^2\theta_W$ affects via equation (7) the vector couplings g_{v_i}, which become a function of s. The *γ–loop–γ* corrections leads to a running and complex $\alpha(s)$. The imaginary part is roughly 1.1% of $\alpha(0)$ [8].

All modifications due to the propagator corrections are absorbed in a "universal" way, thus not depending on initial/final state particles.

(ii) *The Real Part of the Vertex Corrections* can be taken into account by a flavour dependent redefinition of $sin^2\theta_W(s)$ into $sin^2\theta_{W,f}(s)$ and of $g_{a/v}$ into $g_{a/v}(s)$. The latter redefinition is partly due to equation (7) with the new $sin^2\theta_{W,f}(s)$ for g_{v_i}. The additional part is taken into account by a redefinition of $\rho(s)$ into a $\rho_f(s)$, which is now taken as constant factor in front of each $g_{a/v}$ rather than a factor in the coupling strength of the Z^0 exchange part as given in equation (4):

$$\begin{aligned} g_{v_f} &= \sqrt{\rho_f(s)}(I_f^3 - sin^2\theta_{W,f}) \\ g_{a_f} &= \sqrt{\rho_f(s)}I_f^3. \end{aligned}$$

Flavour dependent in this sense means that $\sqrt{\rho_f(s)}$ is different for each quark flavour and different for leptons but equal for all leptons. For the

case of leptons only (as given in this note) the coupling constants are multiplied with a factor of $\sqrt{1.0035}$ [8] for a top mass 150 GeV and a Higgs mass of 200 GeV. The imaginary part of these corrections are small and therefore neglected.

(iii) The Box Corrections are small near the peak and are neglected.

The "QED corrections" are divided into

(i) Kinematic Effects, which account for a shift in x due to initial–, final–state radiation and Bremsstrahlung of the decay product.

(ii) Direct QED Effects, which are essentially a spin flip of the τ. These effects change A_{pol} by -0.0023 and are neglected [3].

The kinematic effects result in a large correction (roughly $5-10\%$) on the polarisation. They are taken into account by a fragmentation model given in [3]. This involves a fourfold convolution. Most of this convolution can be done analytically leaving only one integral. Equation (10) can then be rewritten as

$$\begin{aligned}
\frac{d^2\sigma}{dcos\theta\, dx}(\rho,\delta,\xi;s,cos\theta,x) &= \Big[(1+cos^2\theta)W_0(s,x;\rho)+2cos\theta W_1(s,x;\rho)\Big]+ \\
&\quad \Big[(1+cos^2\theta)W_2(s,x;\delta)+2cos\theta W_3(s,x;\delta)\Big]\,\xi, \\
\text{where } W_i(s,x;\rho/\delta) &= \int_0^{1-x^2}\frac{dv}{\sqrt{1-v}}\rho(v)F_i(s(1-v))H^{\mu}_{(i/2)}(\frac{x}{\sqrt{1-v}};\rho/\delta).
\end{aligned} \tag{11}$$

The function H^{μ}_0 and H^{μ}_1 are general (radiative) cases for the functions h^{μ}_i given in equation (9) and are given in [3], where $\rho(v)$ can be found as well. $\rho(v)$ is the bremsstrahlung distribution, it must not be confused with the Michel parameter ρ or the parameter ρ_0 describing the Higgs sector of the Standard Model. Comparing the structure of equation (11) with the one of (10) it becomes clear that all manipulations due to QED radiative corrections mentioned above *do not change the structure* of the nonradiative equation. Nevertheless it is worth comparing equation (11) with the Born expression (equation 10) w.r.t. the dependence on the production parameters g_{a_e}, g_{v_e}, g_{a_τ} and g_{v_τ} in some detail: Equation (10) at $s = M_Z^2$ depends merely on A_e and A_τ, which are essentially the ratios g_{v_e}/g_{a_e} and g_{v_τ}/g_{a_τ}. This simple behaviour is not conserved going to equation (11) due to the convolution integral which has to take into account the function F_i over the whole range of s and not only at $s = M_Z^2$. Therefore every function W_i depends in principal nontrivially on the parameters g_{a_e}, g_{v_e}, g_{a_τ} and g_{v_τ} itself (and not their ratios). But, having now a closer look to the convolution integral and taking into account that the function $\rho(v)$ in equation (11) shows a $\delta - function$ like behaviour with a sharp maximum at $v = 0$, the main contribution to the integral comes from F_i at $s = M_Z^2$. Therefore the W_i are expected to depend mainly on A_e and A_τ as given in equation (10).

Input			Fit result
Reference value $g_{a_l} = -0.500$		Ref. value $g_{v_e} = -0.040$	
change g_{a_e} by	change g_{a_τ} by	change g_{v_e} by	change in P_τ-
+0.009	-	-	< 0.00005
-	+0.009	-	+0.0002
+0.009	+0.009	-	+0.0002
−0.009	-	-	+0.0003
-	−0.009	-	+0.0001
−0.009	−0.009	-	+0.0008
-	-	+0.048	+0.0023
-	-	−0.045	−0.0010

Table 6: *Change in polarisation varying g_{a_e}, g_{v_e} and g_{a_τ} within reasonable range.*

In other words: If a fit is performed to equation (11) fitting g_{v_e} and g_{v_τ}, while fixing g_{a_e} and g_{a_τ} to some reasonable value, g_{v_e}/g_{a_e} and g_{v_τ}/g_{a_τ} depend only weakly on g_{a_e} and g_{a_τ}. To give a quantitive understanding of this statement a check is performed: Integrating equation (11) over $cos\theta$, a likelihood fit of the momentum spectrum to

$$f(s,x;g_{v_\tau},g_{a_\tau},g_{v_e},g_{a_e}) = \frac{1}{W_0}\left[W_0(s,x;g_{v_\tau},g_{a_\tau},g_{v_e},g_{a_e}) + W_2(s,x;g_{v_\tau},g_{a_\tau},g_{v_e},g_{a_e})\right] \quad (12)$$

is performed extracting A_τ as result (setting ρ, ξ and δ to their "V-A" values). The input reference values are $g_{a_{lepton}} = -0.5$ and $g_{v_{lepton}} = -0.040$, which are very close to the measured values $g_{a_{lepton}} = -0.5029 \pm 0.0041$ and $g_{v_{lepton}} = -0.034\,^{+0.034}_{-0.014}$ in [7]. These measurement errors are used to vary g_{a_τ}, g_{a_e} within more than 2σ. For roughly 8000 Monte Carlo events the results are shown in table 6. It becomes evident that the resulting changes in the structure of equation (8) due to QED radiative corrections are only marginal, and therefore equation (11) is sensitive only to the ratios A_e and A_τ as long as one stays at the peak. Going off the peak, this is not true anymore, so that the g_{a_l} from the measurements of Γ_{ll} have to be used.

4.4 Fit Procedure and Checks with Monte Carlo

As already described in [2], equation (11) is used to calculate a log–likelihood function. The normalised μ momentum and the angle of the identified μ are used. All corrections are taken into account via a momentum and angle dependent efficiency function

$$\epsilon(x,cos\theta) = \epsilon_{Acceptance}(x,cos\theta) \times \epsilon_{\mu-ID}(x,cos\theta) \times (1 + \epsilon_\pi(x,cos\theta) + \epsilon_{\mu\mu}(x,cos\theta)). \quad (13)$$

The individual contributions are explained in sections 3.3, 3.4.1 and 3.4.2.

To check the performance of the method described above a sample of 10000 $\tau \to \mu\nu\nu$ (KORALZ—generator level, momentum not smeared, all radiative effects switched on)

is used. This corresponds roughly to the number of decays expected in the 1991 run. As the fitting methods using equation (11) do—at this stage—not include the resolution effects, nonsmearing is appropriate to check the method. The input values for g_{a_e} and g_{a_τ} are -0.500, those for g_{v_e} and g_{v_τ} are -0.040 ($v/a = 0.079$). This corresponds to a value of -15.6% for the polarisation. The range for $x = E_\mu/E_\tau$ and $cos\theta$ are [0.1;0.95] and [-0.9;0.9] respectively.

Results for different combinations of parameters for the fit to Monte Carlo is shown in table 7. They are discussed now:

- Result (1) shows the fit to the momentum spectrum neglecting the angular information. This corresponds to determining the polarisation only.

- Result (2) shows the extension to the 2–dimensional distribution in momentum and $cos\theta$. g_{v_e}/g_{a_e} can then be measured as well and is found to be in agreement with the expected value. It should be stressed once more that the accuracy for measuring $g_{v_e}/g_{a_e} \approx \frac{1}{2}A_e$ in this case is mainly determined by the term $2cos\theta A_e$ in equation (8), which is linear in A_e, while the measurement of the forward–backward asymmetry allows only a measurement quadratically in A (term $2cos\theta A_e A_\tau$ in equation 8).

- Result (3) demonstrates the opportunity to fit $g_{v_{lepton}}/g_{a_{lepton}}$, assuming lepton universality. The accuracy on $g_{v_{lepton}}/g_{a_{lepton}}$ is slightly higher than the combined error in fit (2) due to a small correlation induced by the term $2cos\theta A_e A_\tau$ in equation (8).

- For result (4) ξ is included as a fit parameter. It shows that equation (10) is quite sensitive to this parameter as well. As the main interest in this context is on the τ sector, g_{v_e} has been fixed to -0.040. For data it can be taken e.g. from the forward–backward asymmetry measurements in the electron channel. The influence of uncertainties in g_{v_e} will be studied in section 5.

- Result (5) shows a combined fit of ξ and ρ, setting g_{v_e} and g_{v_τ} to their Standard Model value. ξ and ρ are found to be consistent with the input values.

- For result (6) the decay parameter ρ is fixed, so that the highest precision w.r.t. the unknown parameter ξ is reached. The value for ρ can be taken from other experiments (e.g. [10]).

- The sensitivity w.r.t. ρ can be seen in result (7), where ξ and δ are fixed to their Standard Model values.

- The same for δ is shown in result (8), where ξ and ρ are fixed to their Standard Model values.

- Result (9) shows the possibility of fitting ξ and ρ simultaneously. Both variables are rather strong correlated.

Fit-Method	*Fit-Results*				
	g_{v_e}/g_{a_e}	g_{v_τ}/g_{a_τ}	ξ	ρ	δ
1) Fit to momentum spectrum (12)	fixed	0.093 ± 0.030	fixed	fixed	fixed
2) Fit to momentum/$cos\theta$ spectrum (11)	0.043 ± 0.028	0.091 ± 0.029	fixed	fixed	fixed
3) As (2), assuming $g_v = g_{v_\tau} = g_{v_e}$	$0.068^{+0.016}_{-0.018}$		fixed	fixed	fixed
4) As (3), fixing $g_{v_e} = -0.040$, fitting ξ as well	fixed	$0.081^{+0.034}_{-0.028}$	$0.95^{+0.37}_{-0.32}$	fixed	fixed
5) As (2), fixing $g_{v_e} = g_{v_\tau} = -0.040$, $\delta = 0.75$, fitting ξ and ρ	fixed	fixed	0.58 ± 0.47	0.819 ± 0.068	fixed
6) As (5), but fixing $\rho = \delta = 0.75$	fixed	fixed	0.96 ± 0.30	fixed	fixed
7) As (5), but fixing $\xi = 1$, $\delta = 0.75$	fixed	fixed	fixed	0.773 ± 0.043	fixed
8) As (5), but fixing $\xi = 1$, $\rho = 0.75$	fixed	fixed	fixed	fixed	0.51 ± 0.29
9) As (5), but fixing $\rho = 0.75$	fixed	fixed	1.57 ± 0.56	fixed	$0.29^{+0.31}_{-0.20}$

Table 7: *Results for check with Monte Carlo.*

Altogether Mote Carlo shows that the (semi–)analytical approach reproduces the input parameters.

5 Results and Systematic Effects

Several possibilities of measurements have been presented in the last section. In this chapter the two–dimensional distribution is used to fit either g_{v_e}/g_{a_e} and g_{v_τ}/g_{a_τ} simultaneously or g_v/g_a assuming lepton universality. The third measurement is the simultaneous determination of g_{v_τ}/g_{a_τ} and ξ, fixing ρ to it's measured value 0.731 ± 0.030 [10] assuming $\delta = 0.75$ (which corresponds to "V-A" or "V+A" at both vertices of the W in the τ decay). For all combinations systematic studies have been performed as explained in [2] taking the variations with angle into account. This has been done by varying the relevant distribution/number in each detector bin separately.

The corresponding systematic errors for each measurement are given in table 8. For the theoretical error it has been assumed that the QED radiative corrections are known to 20%, which is a conservative estimate.

To show the quality of the fit, figure 9 shows the projection onto $cos\theta$ and x_μ for the data together with the best fit.

5.1 Determination of g_{v_e}/g_{a_e} and g_{v_τ}/g_{a_τ}

For this measurement the τ decay parameter are set to their Standard Model value ("V-A") as done for the polaristaion analysis of the μ channel in [11]. The input values $g_{a_e} = -0.5014 \pm 0.0029$ and $g_{a_\tau} = -0.487 \pm 0.012$ are taken from the most recent fit to the asymmetries and the line–shapes [8]. The result for the ratio of vector and axialvector couplings is

$$\begin{aligned} \frac{g_{v_e}(s = M_Z^2)}{g_{a_e}(s = M_Z^2)} &= 0.110\,^{+0.064}_{-0.054_{stat}} \pm 0.019_{syst}, \\ \frac{g_{v_\tau}(s = M_Z^2)}{g_{a_\tau}(s = M_Z^2)} &= 0.119\,^{+0.060}_{-0.053_{stat}} \pm 0.031_{syst}. \end{aligned} \tag{14}$$

The last number can be translated into a τ polarisation of $P_{\tau^-} = (-23.5^{+10.2}_{-11.5})\%$, which compares well with $(-19.2 \pm 12.9)\%$ in [11]. The improvement in the error is due to the additional information from the angle and the increased statistics. The measurement of the ratio of the electron couplings can be compared to the value obtained from the forward–backward asymmetries [8]: $g_{v_e}(s = M_Z^2)/g_{a_e}(s = M_Z^2) = 0.070 \pm 0.028$. The corresponding result for the couplings of the τ are $g_{v_\tau}(s = M_Z^2)/g_{a_\tau}(s = M_Z^2) = 0.220 \pm 0.105$. They are in good agreement. It should be stressed that the main contribution to the sensitivity w.r.t. g_{v_e} comes from the term $2A_e cos\theta$ in equation (8). Usually this term is called the forward–backward polarisation asymmetry $A_{FB}^{pol} = -\frac{3}{4}A_e$.

5.2 Determination of $g_{v_{lepton}}/g_{a_{lepton}}$

Due to the correlation between the electron and τ couplings one can gain a little bit more than the usual $\sqrt{2}$ for the assumption of lepton universality. As input $g_{a_{lepton}} = -0.4988 \pm 0.0021$ is used, which has been obtained by the line-shape and asymmetry fit assuming lepton universality [8]. The result is

$$\frac{g_{v_{lepton}}(s = M_Z^2)}{g_{a_{lepton}}(s = M_Z^2)} = 0.114\,^{+0.030}_{-0.034_{stat}} \pm 0.016_{syst}. \tag{15}$$

This can be compared to the fits to the asymmetries for lepton universality, which lead to $g_{v_{lepton}}(s = M_Z^2)/g_{a_{lepton}}(s = M_Z^2) = 0.082 \pm 0.016$. They are in good agreement.

5.3 Determination of g_{v_τ}/g_{a_τ} and ξ

From the measurements of the asymmetries and the width Γ_{ee}, g_{v_e} and g_{a_e} are fixed to $g_{v_e} = -0.035 \pm 0.014$ and $g_{a_e} = -0.5014 \pm 0.0029$. The angular information is then used to distinguish between ξ and g_{v_τ}/g_{a_τ} (or the τ polarisation P_τ-). This is very interesting, because the usual determination of the polarisation of the τ is the measurement of the product $\xi \times P_\tau$-. One of the two other decay parameters ρ and δ is fixed by other measurements to $\rho = 0.731 \pm 0.030$ [10]. Unfortunately, the present statistics does not allow to fit the remaining δ and ξ simultaneously. So, the measurement of ξ can only be given under the assumption of $\delta = 3/4$ or some other fixed value.

A restriction to $\delta = 3/4$ makes sense, as it has some power in distinguishing between "V-A" and "V+A" in the charged current. As already said before (see table 5), "V-A" at both vertices leads to $\xi = 1$, while "V+A" at both vertices results in $\xi = -1$. For both cases δ is predicted to be 3/4.

Two procedures are possible: Fitting g_{v_τ}/g_{a_τ} and ξ simultaneously disregarding any other measurements in ALEPH, or using the measurement of $A_\tau^{FB} = 0.0438 \pm 0.0144$ from the asymmetries [8] as a constraint. As the main interest is the measurement of ξ, the constraint is used. This guarantees the correct treatment of the correlation of g_{v_τ}/g_{a_τ} and ξ getting the maximum information on ξ. Clearly the measurement of g_{v_τ}/g_{a_τ} in this method is dominated by the constraint. The result is

$$\xi = 0.72\,^{+0.52}_{-0.34_{stat}} \pm 0.30_{Uncert.\ on\ g_{v_e},\rho} \pm 0.18_{syst},$$

$$\frac{g_{v_\tau}(s = M_Z^2)}{g_{a_\tau}(s = M_Z^2)} = 0.201\,^{+0.073}_{-0.069_{stat}}\,^{+0.154}_{-0.056_{Uncert.\ on\ g_{v_e},\rho}} \pm 0.015_{syst}. \tag{16}$$

Some comment should be given for the systematic error due to the uncertainty in g_{v_e}:
The large systematic error on g_{v_τ}/g_{a_τ} for the constrained fit is simply the fact that due to the constraint the product $g_{v_\tau} \times g_{v_e} \propto A_{FB}^\tau$ is demanded to be more or less constant. Thus, a variation of g_{v_e} to lower values results in a larger value for g_{v_τ}/g_{a_τ} and vice versa. But most important is the fact that the influence on ξ is substantially smaller compared to the unconstrained fit.

For comparison the result of the unconstrained fit is given as well:

$$\xi = 1.22\,^{+1.43}_{-0.79\,stat}\,^{+0.81}_{-0.15\,Uncert.\ on\ g_{v_e},\rho} \pm 0.25_{syst},$$

$$\frac{g_{v_\tau}(s=M_Z^2)}{g_{a_\tau}(s=M_Z^2)} = 0.117\,^{+0.165}_{-0.072\,stat}\,^{+0.020}_{-0.052\,Uncert.\ on\ g_{v_e},\rho} \pm 0.26_{syst}.$$

The unconstrained fit itself is quite sensitive to g_{v_e} as well. But in this case a large fluctuation of ξ to higher values corresponds to a large fluctuation of g_{v_τ}/g_{a_τ} to lower values. This can be understood in terms of the high correlation between these two quantities in the unconstrained fit. Especially the fluctuation of g_{v_e} to lower values causes severe problems for the fit due to this high correlation. The value given in the table corresponds therefore to the variation of -0.75σ in g_{v_e} rather than -1σ.

Rather soon the accuracy on g_{v_e} can be improved by higher statistic and/or taking other (LEP) experiments into account leading to a smaller uncertainty in ξ and g_{v_τ}/g_{a_τ}.

6 Conclusions

The two–dimensional energy/angle distribution of μ from τ decays has been used to extract several combinations of parameters. It is now possible to draw some conclusions from the different measurements. One interesting quantity is clearly the Weinberg angle. The best measurement in this context can be obtained from result (15) assuming lepton universality (-0.0007 is the flavour dependend correction as described in 4.3):

$$sin^2\theta_W(s=M_Z^2) = \frac{1}{4}\left(1 - \frac{g_{v_{lepton}}(s=M_Z^2)}{g_{v_{lepton}}(s=M_Z^2)}\right) - 0.0007 = 0.2208 \pm 0.0089. \qquad (17)$$

The simultaneous determination of electron and τ couplings as described in result (14) corresponds to the simultaneous measurement of the polarisation *and* of the forward–backward asymmetry of the polarisation. Comparing the error on g_{v_τ}/g_{a_τ} with the measurement from energy only one gains roughly 13% in the statistical error. In addition one gets a new determination of g_{v_e}/g_{a_e}. As this measurement is linear in g_{v_e}/g_{a_e}, the sensitivity is only $\approx 30\%$ worse compared to the sensitivity for the determination from the forward–backward asymmetry for the e^+e^- final state. Consequently, doing this analysis in a similar manner with the other τ decay channels can increase the sensitivity on g_{v_e}/g_{a_e} substantially.

The determination of ξ and g_{v_τ}/g_{a_τ} with the constraint from the forward–backward asymmetry is the first measurement of ξ. Although the result still depends on the value for δ, the sensitivity is remarkable. Even with the restriction $\delta = 3/4$ the value of ξ still allows to distinguish between "V-A" and "V+A" at both vertices of the W. Result (16) excludes the "V+A" ($\xi = -1$) combination by more than 3σ.

Source	*Systematic Error on*			
	$\frac{g_{v_\tau}}{g_{a_\tau}}$ $\frac{g_{v_e}}{g_{a_e}}$	$\frac{g_{v_{lepton}}}{g_{a_{lepton}}}$	ξ $\frac{g_{v_\tau}}{g_{a_\tau}}$ unconstrained	ξ $\frac{g_{v_\tau}}{g_{a_\tau}}$ constrained
Acceptance	0.015 0.008	0.007	0.08 0.008	0.09 0.006
μ–Id (slope)	0.007 $\approx 0.$	0.004	0.07 0.005	0.06 0.001
μ–pre–Id (height)	0.001 0.003	0.002	0.06 0.008	$\approx 0.$ 0.008
x_{recoil} cut	0.013 0.007	0.006	0.12 0.011	0.05 0.007
$\tau \rightarrow$ *hadron* bckgrd	0.015 0.006	0.007	0.16 0.009	0.11 0.007
2γ bckgrd	0.010 0.008	0.006	0.04 0.013	0.06 0.004
Experimental syst. error (1)	0.028 0.015	0.014	0.24 0.023	0.17 0.015
Uncertainty in $g_{a_{lepton}}$	*not relevant*	0.001	*not relevant*	*not relevant*
Uncertainty in g_{v_e}	*not relevant*	*not relevant*	$^{+0.80}_{-0.05}$ $^{+0.005}_{-0.048}$	0.28 $^{+0.154}_{-0.056}$
Uncertainty in g_{a_e}	0.001 0.001	*not relevant*	0.08 0.009	$\approx 0.$ 0.001
Uncertainty in g_{a_τ}	0.002 0.001	*not relevant*	0.04 0.005	$\approx 0.$ $\approx 0.$
Uncertainty in ρ	*not relevant*	*not relevant*	0.11 0.016	0.10 0.001
Uncertainties of parameters (2)	0.002 0.001	0.001	$^{+0.81}_{-0.15}$ $^{+0.020}_{-0.052}$	0.30 $^{+0.154}_{-0.056}$
Theoretical Uncertainties (QED radiative corr.) (3)	0.012 0.012	0.007	0.06 0.012	0.06 0.002
Total systematic error (1) $\oplus$ (2) $\oplus$ (3)	0.031 0.019	0.016	$^{+0.85}_{-0.29}$ $^{+0.033}_{-0.058}$	0.35 $^{+0.155}_{-0.058}$

Table 8: *Systematic errors for the different measurements*

References

[1] St. Roehn, Ph.D. thesis (Mainz), in preparation.

[2] St. Roehn, A. Stahl, ALEPH-note 90–26 (PHYSIC 91–25).

[3] G. Altarelli et al. (editors), Z Physics at LEP, **CERN 89-08 Volume 1** (1989) 235-265; and *Erratum* from 8 March 1990;
(The sign for p given in equation 2.1 is wrong).

[4] G. Altarelli et al. (editors), Z Physics at LEP, **CERN 89-08 Volume 1** (1989) 7-54.

[5] G. Altarelli et al. (editors), Z Physics at LEP, **CERN 89-08 Volume 1** (1989) 203-234.

[6] D.C. Kennedy, B.W. Lynn, **SLAC-PUB 4039** (1986, revised 1988).

[7] D. Decamp et al. (ALEPH Collaboration), *Z. Phys. C — Particles and Fields* **48** (1990) 365.

[8] M. Martinez, private communication.

[9] F. Scheck, *Phys. Rep.* **44** (1978) 187-248.

[10] Number given at the Orsay τ workshop, Sept. 1990 by the ARGUS collaboration, averaged with the world average given in Particle Data Group *Phys. Lett.* **B239** (1990).

[11] Measurement of the Polarization of τ Leptons Produced in Z^0 Decays, to be puplished, first draft available.

7 Figures

Figure 1: CLPPLN distribution for Barrel and Endcap, section 3.2. μ testsample 1 in [2]; π testsample 4 in [2]; both after penetration cut M1

Figure 2: Efficiency for μ–identification for the different detector bins, section 3.2.

Figure 3: Efficiency for μ–pre–identification for the different detector bins, section 3.2.

Figure 4: Acceptance and Resolution for the different detector bins, section 3.3.

Figure 5: π misidentification probability versus momentum for the full detector, subsection 3.4.1.

Figure 6: Spectra of π background for the different detector bins, section 3.4.1.

Figure 7: Spectra for μ–pair background for the different detector bins, section 3.4.2.

Figure 8: Spectra for signal together with μ–pair and π background for the different detector bins, section 3.5.

Figure 9: Projection onto $cos\theta$ and x_μ for the data together with best fit, section 5.

CLPPLN for Mu and Pi

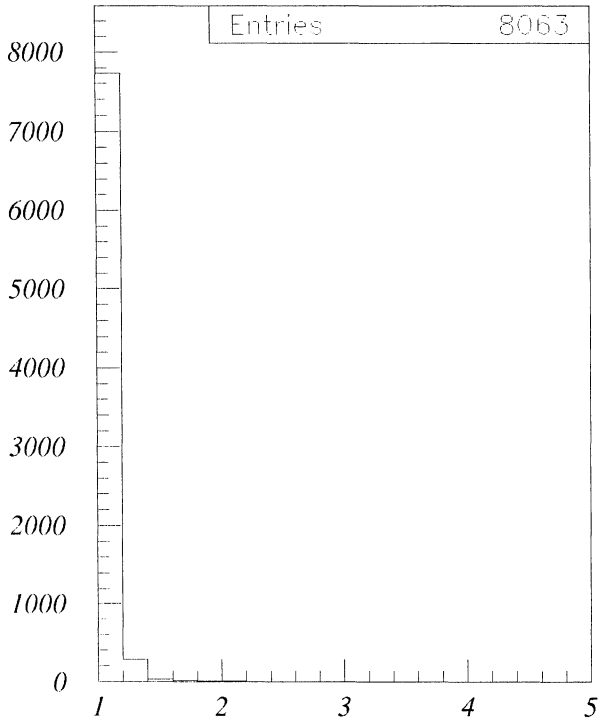

CLPPLN - BARREL - MU

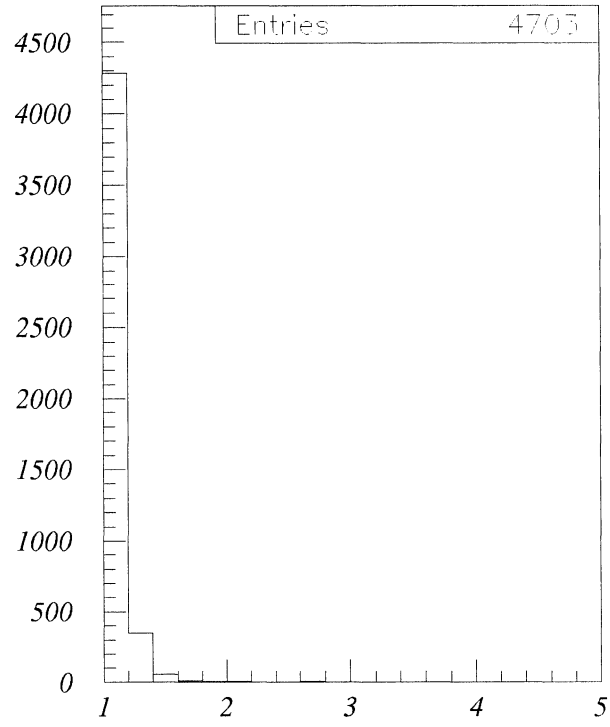

CLPPLN - ENDCAP - MU

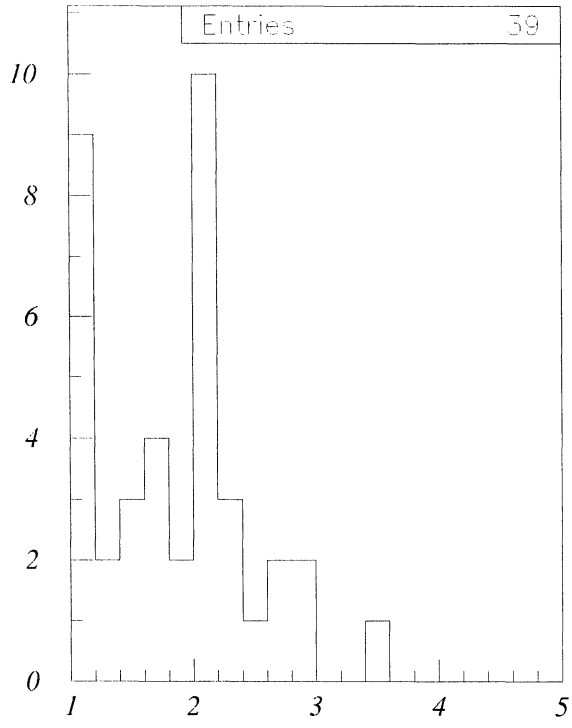

CLPPLN - BARREL - PI

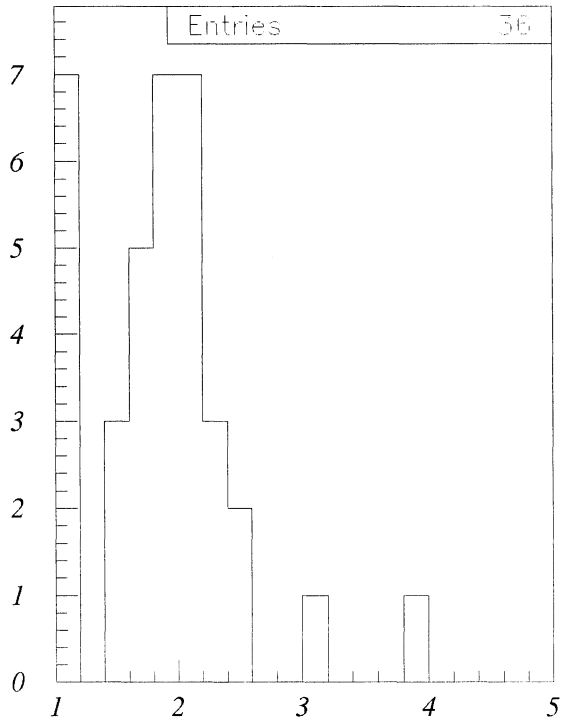

CLPPLN - ENDCAP - PI

Fig. (1)

MUON-ID - Signal - ch-tag

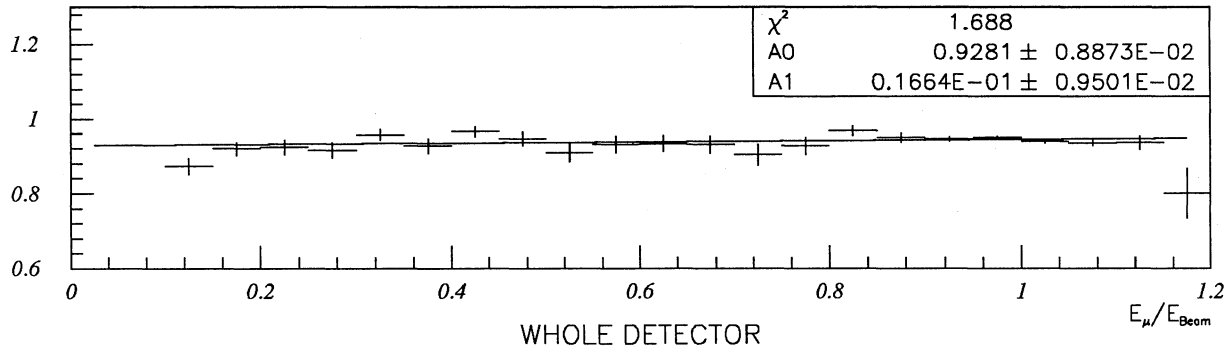

WHOLE DETECTOR

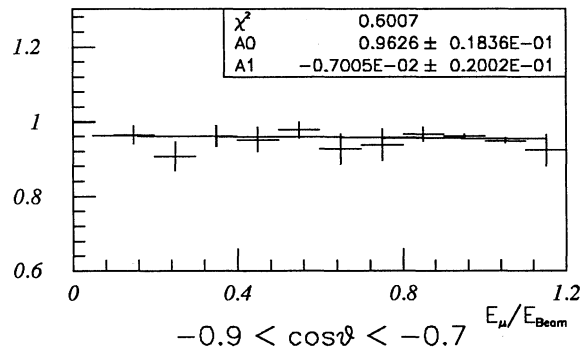

$-0.9 < \cos\vartheta < -0.7$

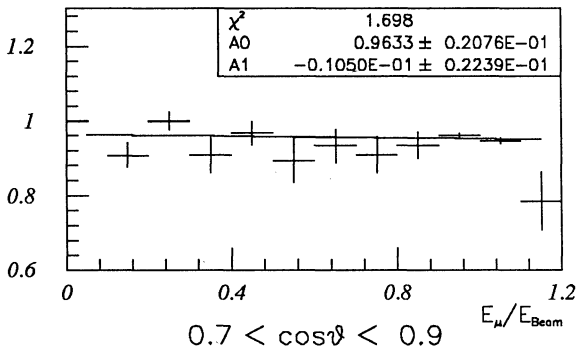

$0.7 < \cos\vartheta < 0.9$

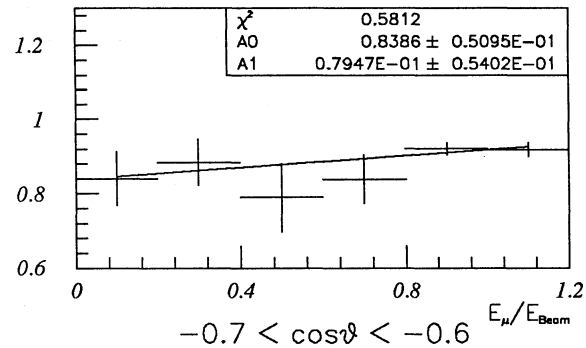

$-0.7 < \cos\vartheta < -0.6$

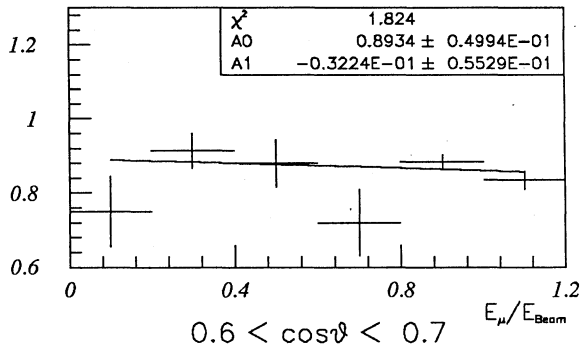

$0.6 < \cos\vartheta < 0.7$

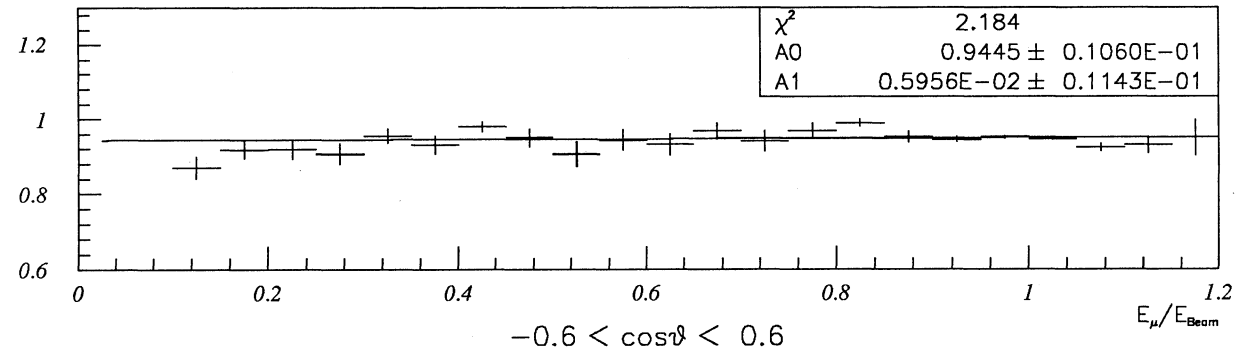

$-0.6 < \cos\vartheta < 0.6$

Fig. (2)

MUON-ID - Background - ch-tag

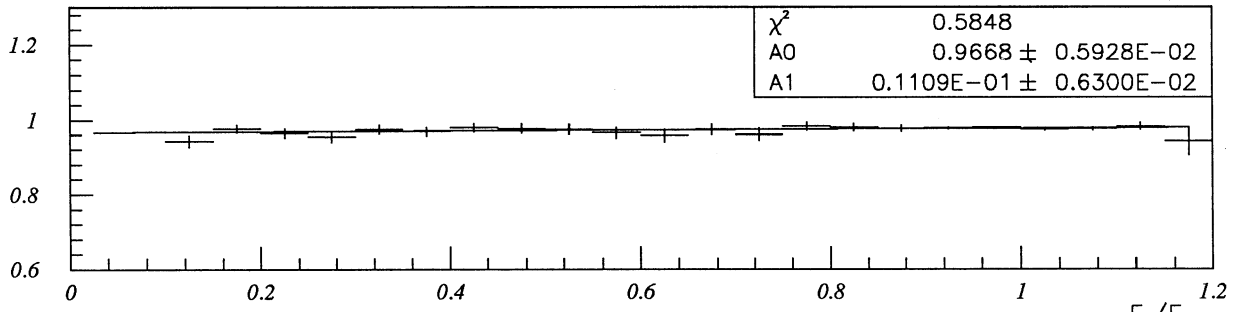

WHOLE DETECTOR

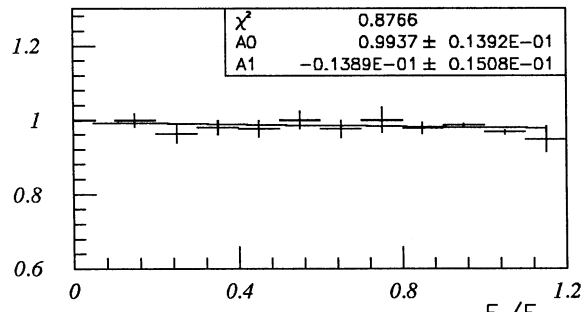

$-0.9 < \cos\vartheta < -0.7$

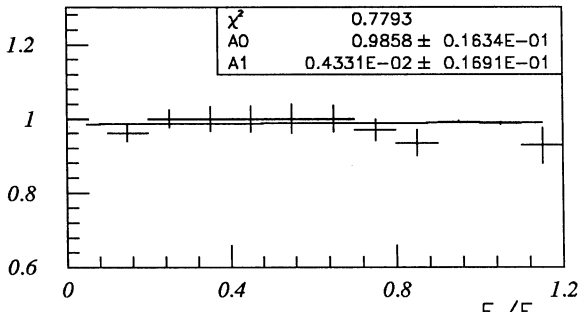

$0.7 < \cos\vartheta < 0.9$

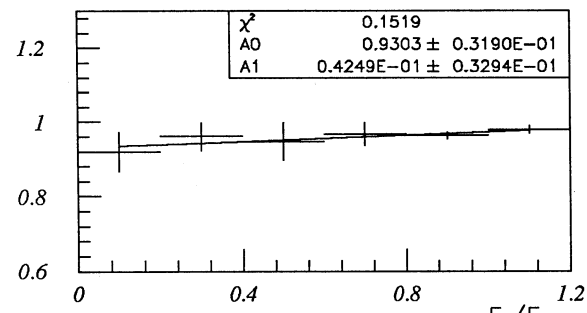

$-0.7 < \cos\vartheta < -0.6$

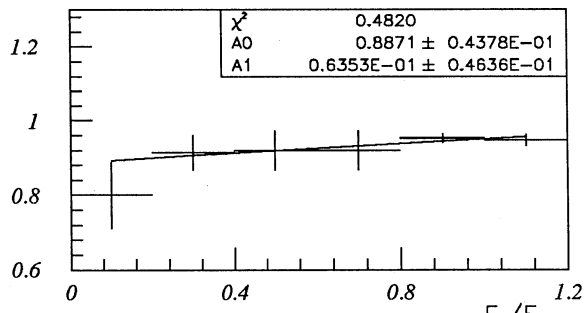

$0.6 < \cos\vartheta < 0.7$

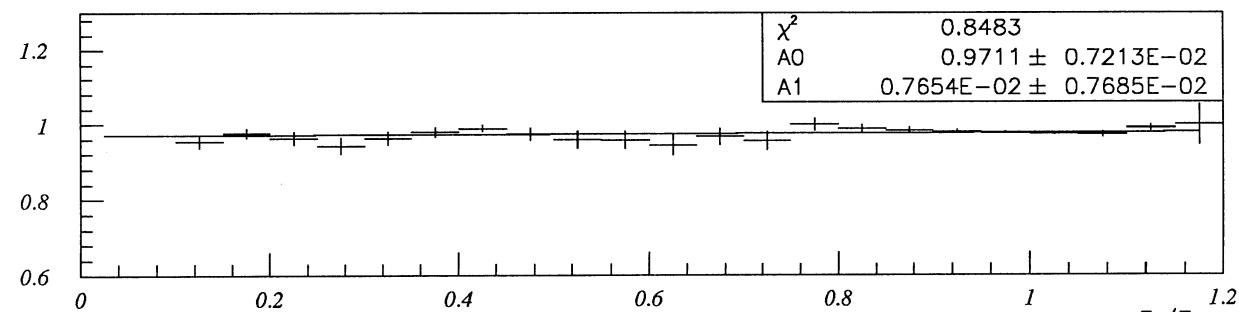

$-0.6 < \cos\vartheta < 0.6$

Fig (3)

Acceptance and Resolution Corrections

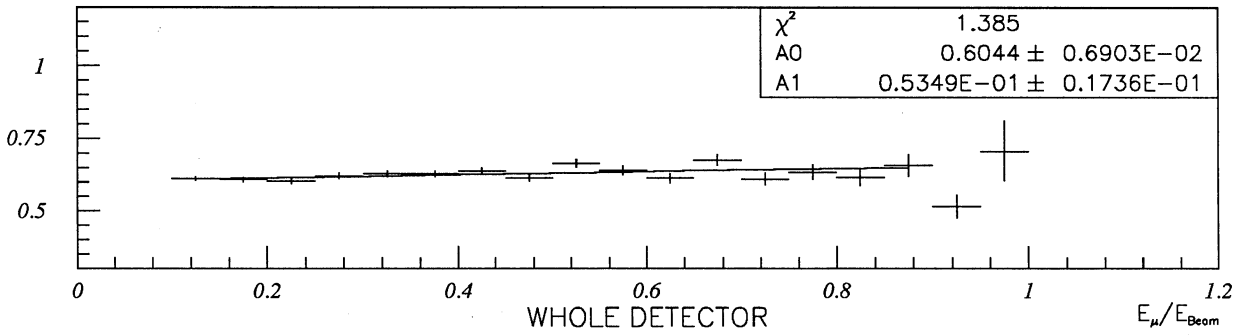

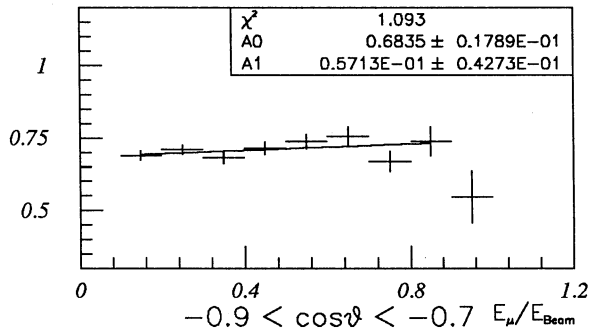

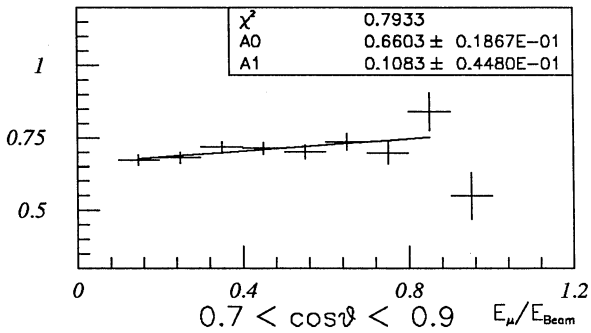

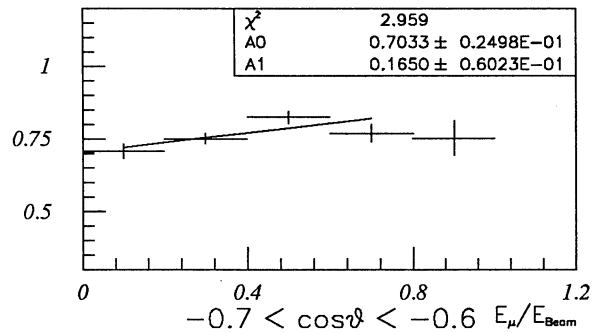

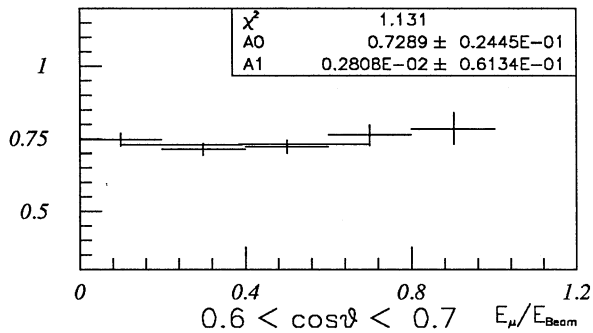

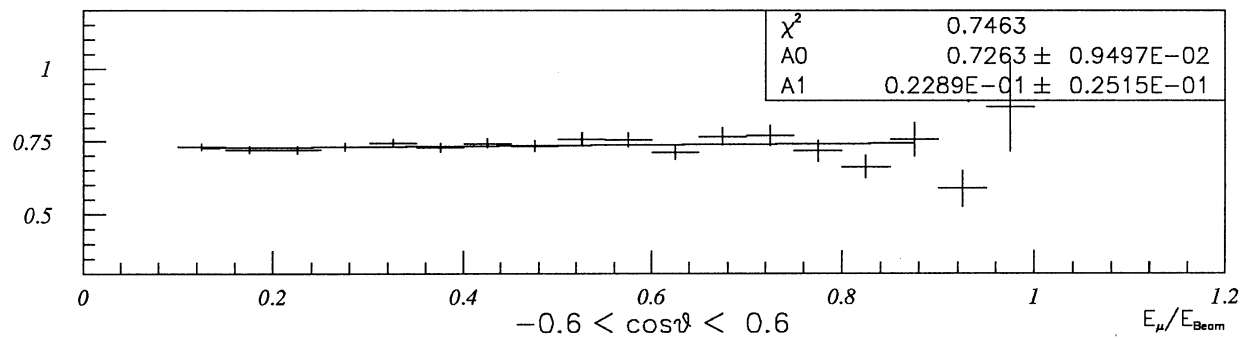

Fig (4)

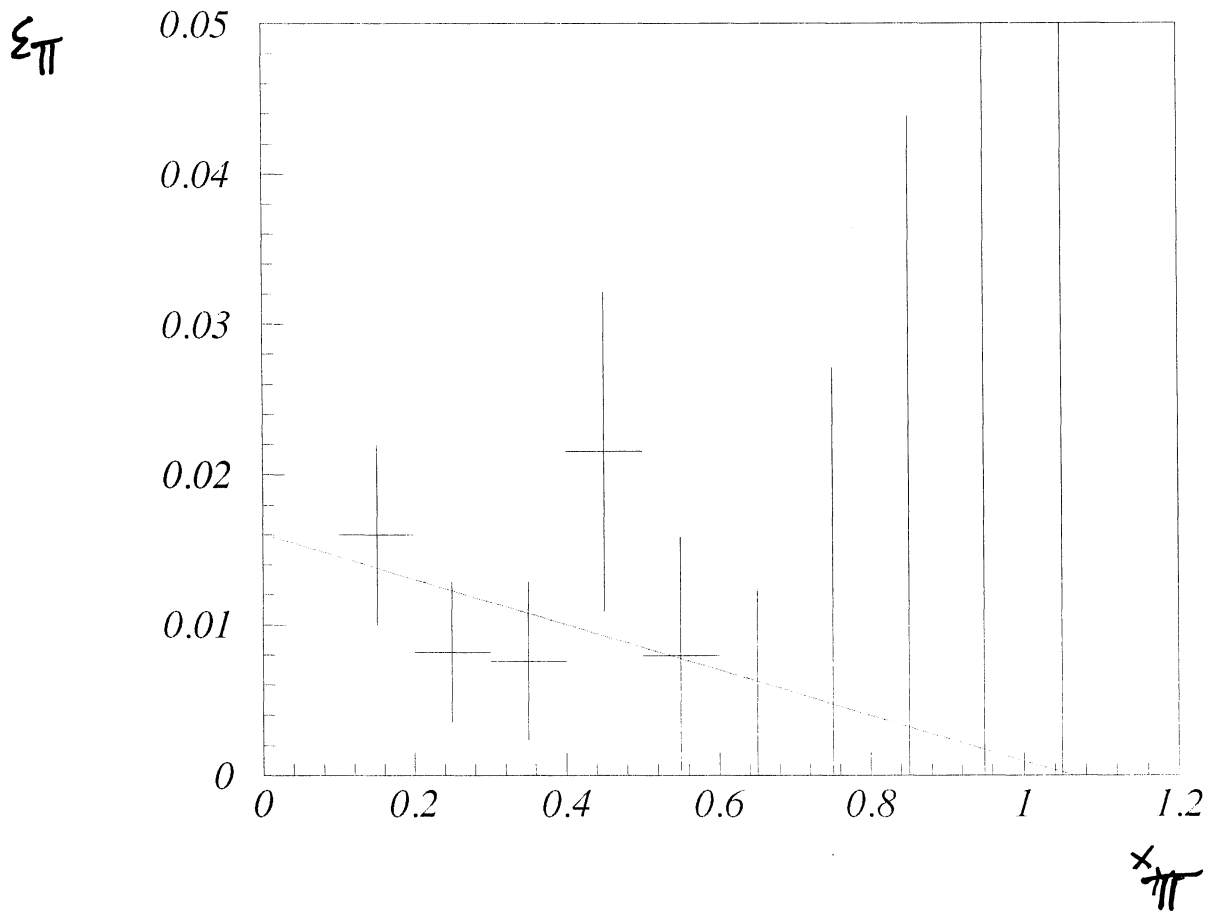

Fig. (5)

Pion - Background

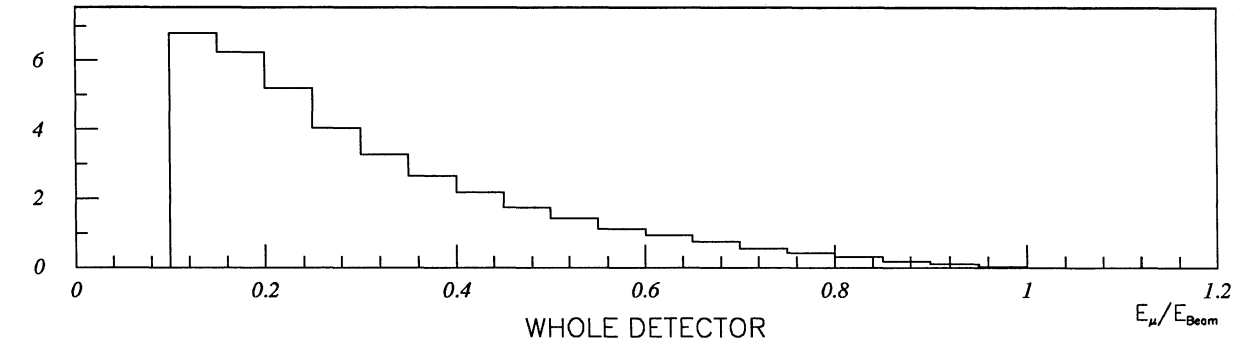

WHOLE DETECTOR

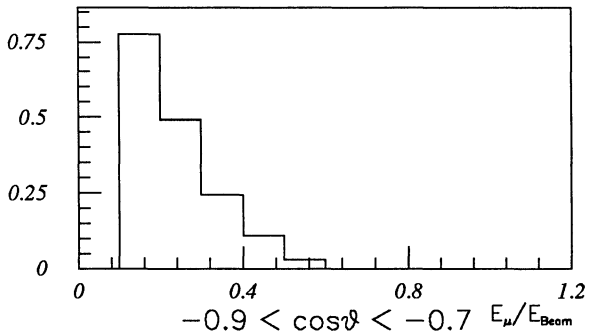

$-0.9 < \cos\vartheta < -0.7$

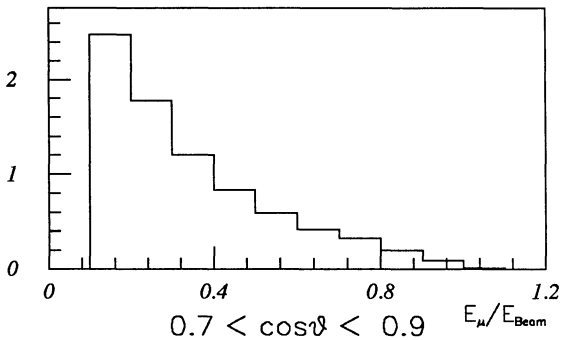

$0.7 < \cos\vartheta < 0.9$

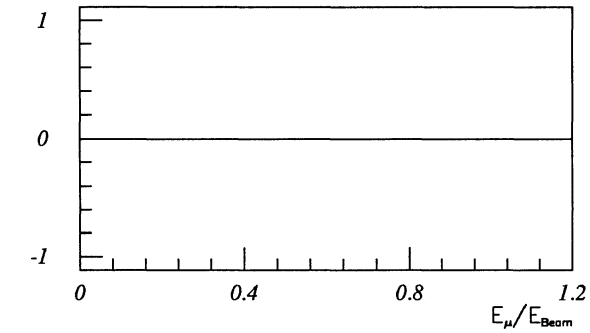

$-0.7 < \cos\vartheta < -0.6$

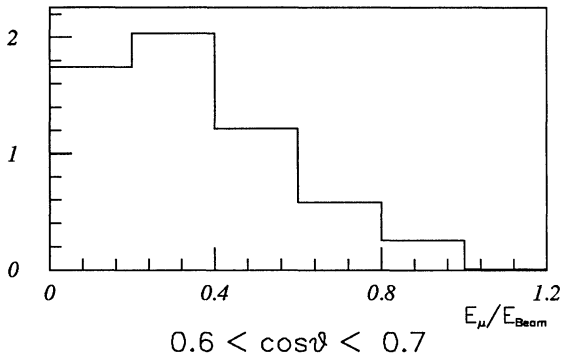

$0.6 < \cos\vartheta < 0.7$

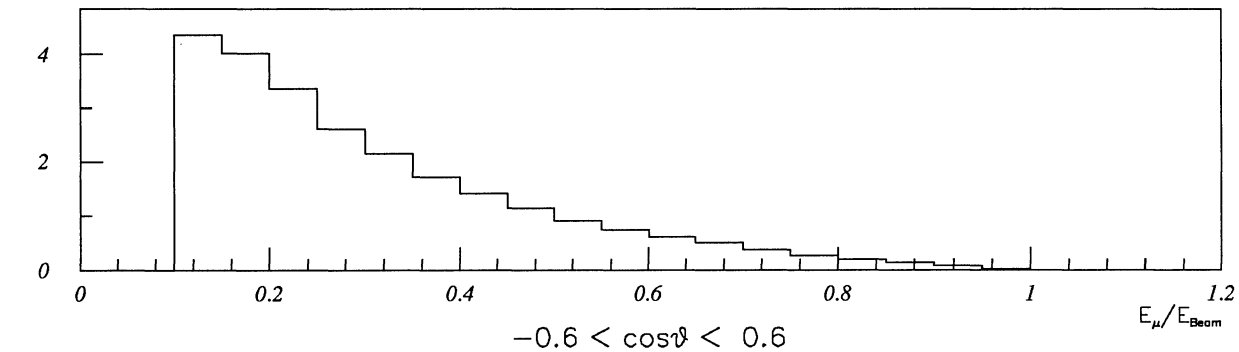

$-0.6 < \cos\vartheta < 0.6$

Fig. 6

Mumu - Background

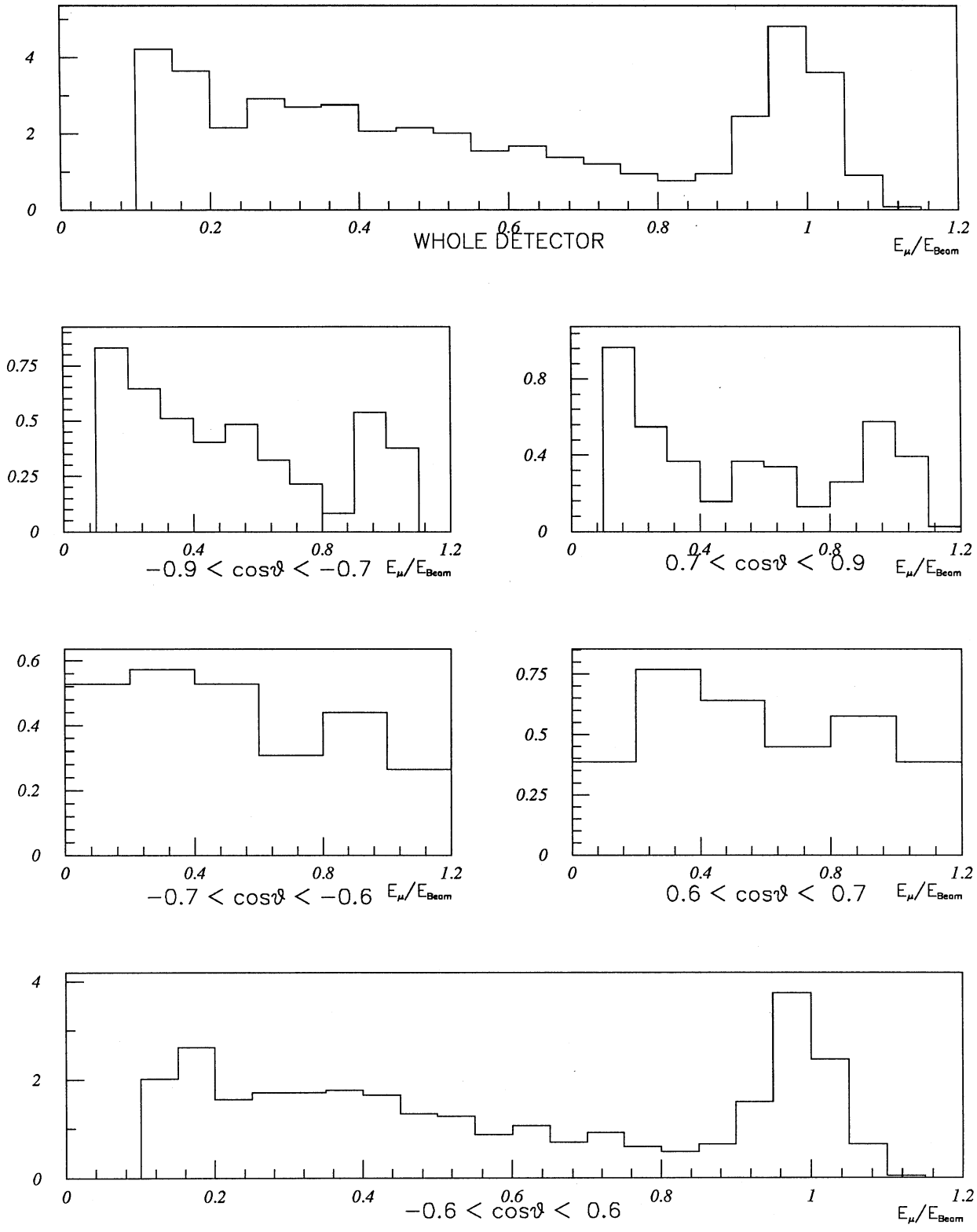

Fig. 7

Mu - spectra with background

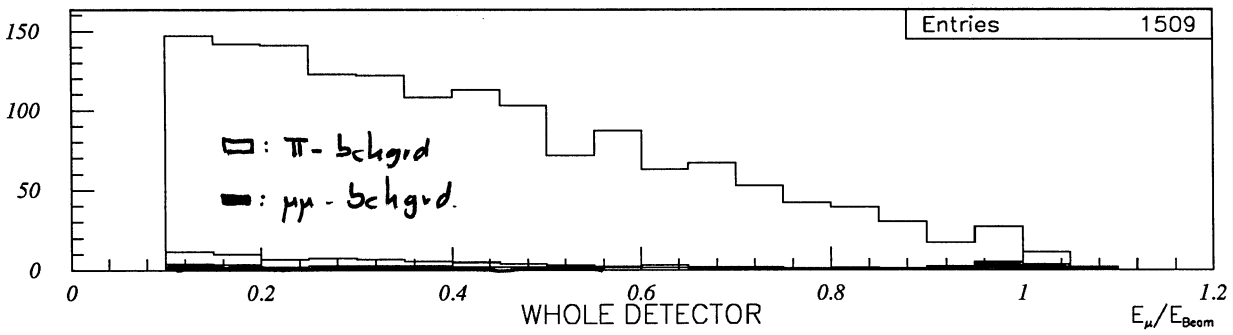

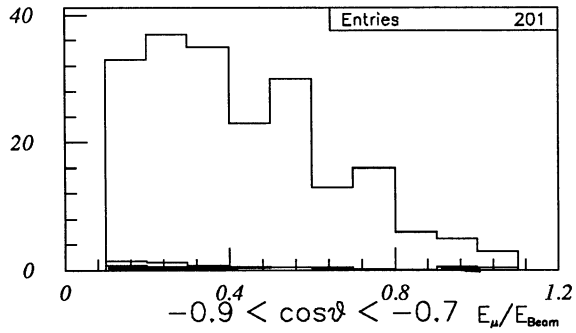

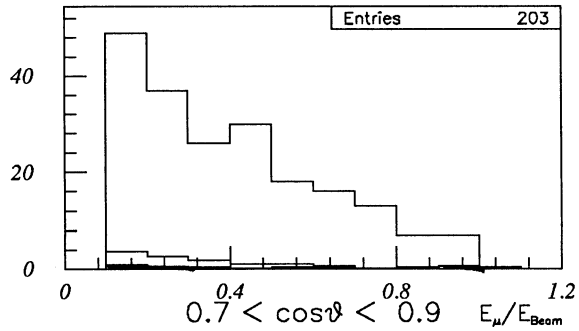

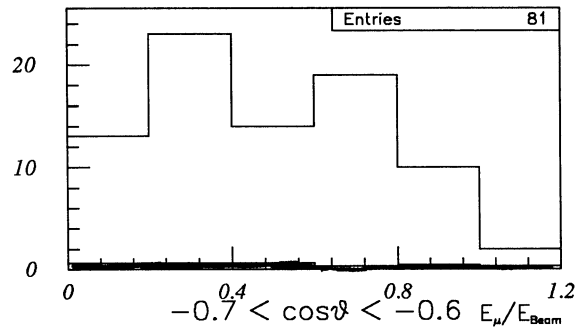

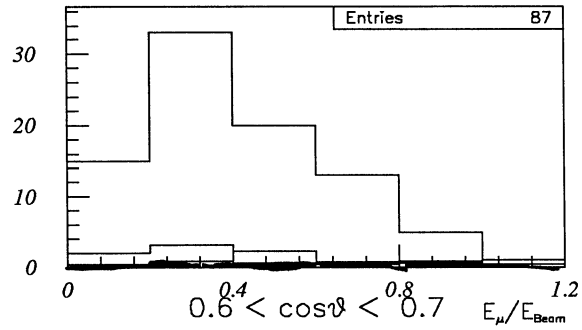

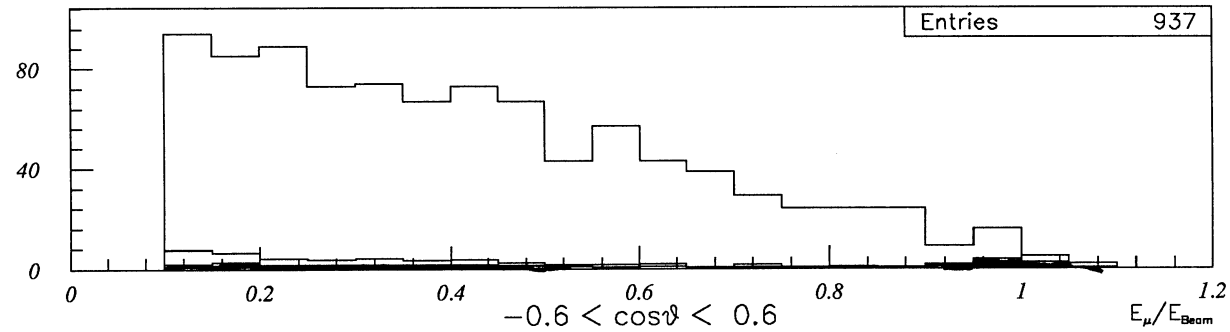

Fig. (8)

Fit Result

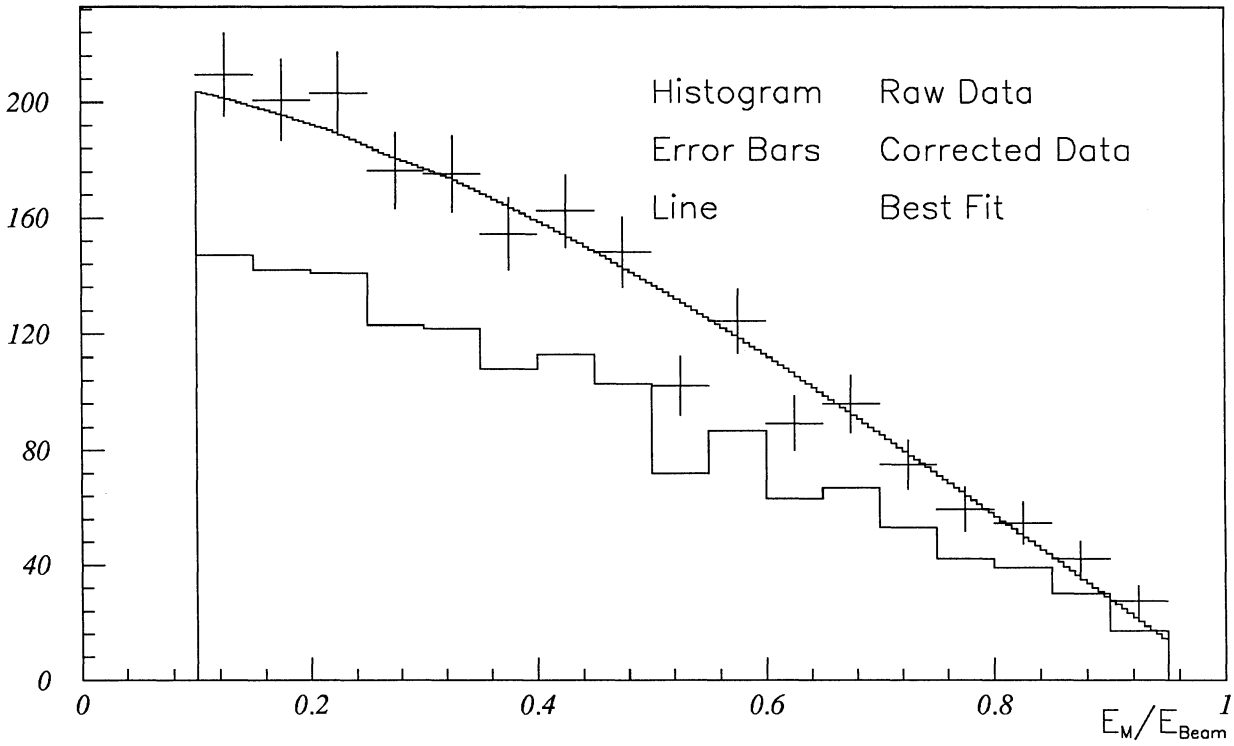

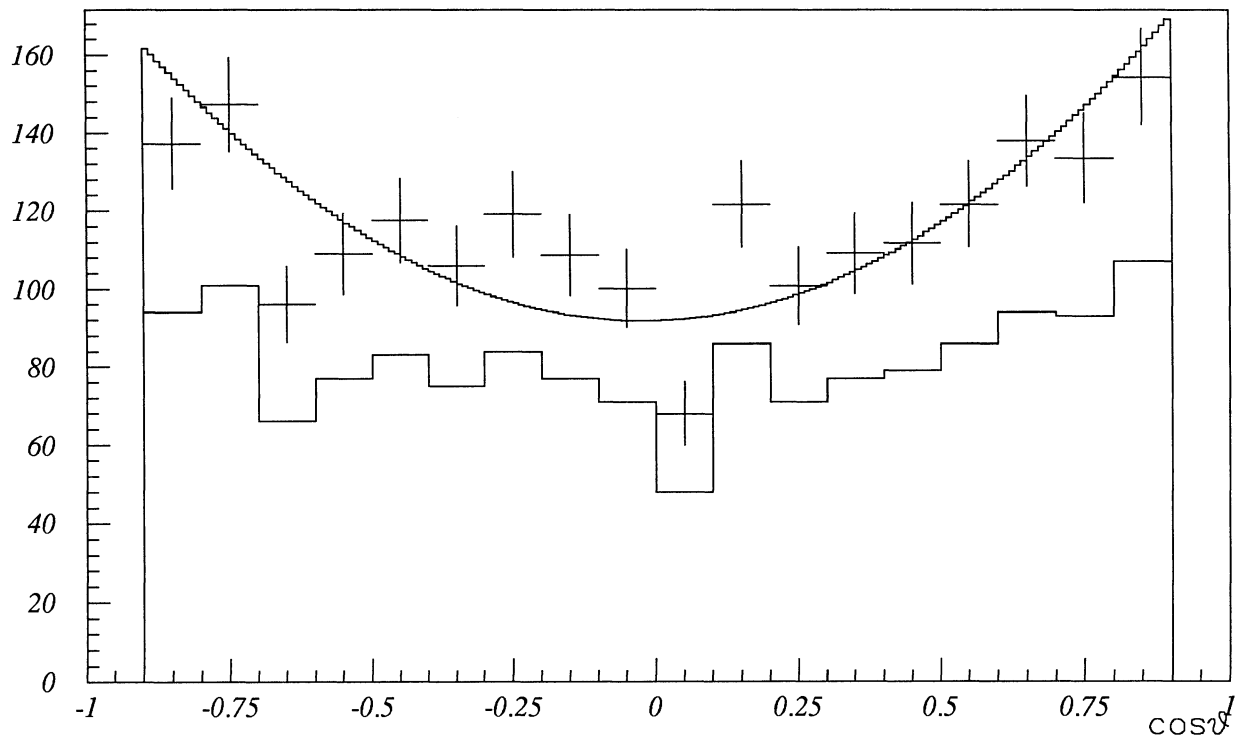

Fig. 9